IEEE Access
Multidisciplinary | Rapid Review | Open Access Journal

Received 10 March 2024, accepted 16 April 2024, date of publication 29 April 2024, date of current version 10 May 2024.

Digital Object Identifier 10.1109/ACCESS.2024.3395124

RESEARCH ARTICLE

Broadband DRA With Uniform Angular Dependent Delay for Indoor Localization

ALI RASHIDIFAR[1], FLORIAN RÖMER[2], (Senior Member, IEEE), SEBASTIAN SEMPER[1], NAM GUTZEIT[3,4], AND GIOVANNI DEL GALDO[1], (Member, IEEE)

[1]Electronic Measurements and Signal Processing Group, Technische Universität Ilmenau, 98693 Ilmenau, Germany
[2]Fraunhofer Institute for Nondestructive Testing IZFP, 66123 Saarbrücken, Germany
[3]eCeramix GmbH, 98693 Ilmenau, Germany
[4]Institute of Micro- and Nanotechnologies, MacroNano Electronics Technology Group, Technische Universität Ilmenau, 98693 Ilmenau, Germany

Corresponding author: Ali Rashidifar (ali.rashidifar@tu-ilmenau.de)

This work was conducted under "The Prime Project," which was funded by the Carl-Zeiss Foundation.

ABSTRACT Estimating the Time Difference of Arrival (TDoA), is a simple yet reliable technique to accurately perform an indoor monostatic localization. To implement TDoA estimation, one approach is to utilize a broadband radar system equipped with multiple receiving antenna elements. To obtain the Time of Arrival (ToA) at each antenna element, the round-trip time is required. However, the round-trip time does not only consist of the propagation delay in free space but the propagation delay within the antenna as well. To perform the localization precisely, it is desired that an antenna element introduces a uniform delay in all directions. To this end, a compact rectangular dielectric resonator antenna is designed for the operating frequency of 6.5 GHz with a fractional bandwidth of 20%. Al_2O_3 with a dielectric constant of 9.8 is used for the substrate as well as the dielectric resonator. The antenna is designed to provide a high correlation between the input and the output pulses. To investigate the correlation, the antenna is excited with a modulated Gaussian pulse and the radiated pulses are studied. The antenna possesses an excellent behavior in terms of pulse preservation for the upper hemisphere. Therefore, when incoming pulses from the same distance but different directions impinge on the antenna, they reach the port of the antenna at a similar time. It is shown that this feature of the proposed antenna allows the utilization of TDoA estimation without the need for a calibration step. The characteristics of the antenna are verified by simulation and measurement.

INDEX TERMS Angular dependent delay, broadband, dielectric resonator antenna, indoor localization.

I. INTRODUCTION

Localization is a crucial requirement for those applications where the awareness of the surrounding environment is important such as service robots [1]. Recently, the use of these types of robot in an indoor environment has become very popular. For such a robot to operate properly, it is necessary to know the positions of the objects relative to its location.

To perform indoor localization using a radar system is a common practice. The reason for that is with having a high bandwidth (BW) a high spatial resolution can be obtained. For example, with a BW of 1.5 GHz an accuracy in the range of a few centimeters can be obtained at a moderate SNR. In addition to that, since the information is spread over a wide range of frequencies, the required transmitting power can be low. This enables the use of broadband signals in an indoor area without causing interference to other devices [2].

Figure 1 illustrates a scenario where a service robot transmits pulses in all directions and receives the echoes with more than one receiving antennas. When knowing the times of transmission and reception, the round trip times can be obtained. Then, the distance to the object and Direction of Arrival (DoA) can be estimated using TDoA.

In an ideal case, the Transmit Antenna (Tx) and Receive Antenna (Rx) of the robot do not contribute to the round trip time. However, this is not the case in practice. Generally,

The associate editor coordinating the review of this manuscript and approving it for publication was Debabrata K. Karmokar.

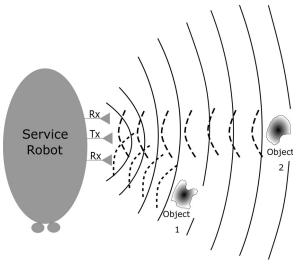

FIGURE 1. A service robot detecting the surrounding objects by using a radar system.

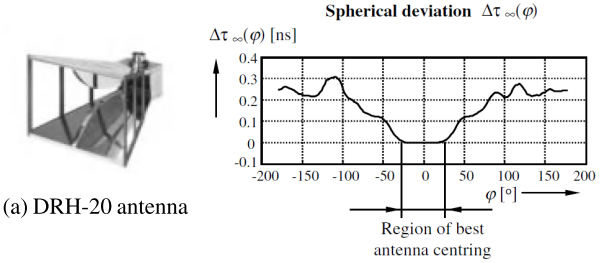

(a) DRH-20 antenna

(b) Estimated delay in azimuth cut

FIGURE 2. DRH-20 and its normalized ADD (The result is taken from page 426 of [4]).

broadband antennas, do not have a uniform transient behavior in the angular domain. To elaborate, if an antenna is placed in the center of a sphere, the radiated pulses from the antenna do not reach different observation points on the surface of the sphere, at the same time. This is true for the receiving mode as well – if the pulses are transmitted from different angles on the surface of the sphere at the same time, they reach the port of the antenna at different time instants. In [3] this characteristic is referred to as the Angular Dependent Delay (ADD). Sachs in [4, Ch. 4.6.3] has provided the ADD measurement result of a DRH-20 antenna for a single azimuth cut. The result is shown in Figure 2b. It can be seen that the antenna has a uniform ADD near the boresight of the antenna, ±25°. However, this is not the case for the angles beyond the boresight region.

To investigate the impact of a non-ideal antenna on the round trip time, assume the DRH-20 is used as the Rx for the robot in Figure 1. Object 1 is closer to the robot compared to object 2. However, the reflected pulse from object 1 experiences an extra delay, since the Rx contributes an extra delay in that direction.[1] This results in having a wrong distance calculation to the object 1, and eventually, wrong DoA estimate.

However, if an antenna has a uniform ADD for the complete field-of-view, it introduces the same delay in all directions. This results in omitting a calibration step. Therefore, it is desired to have an antenna which possesses a uniform ADD over a wide field of view.

There has been a considerable number of investigations on performance of broadband antennas in terms of angular dependency. Characteristics of Ultra Wideband (UWB) antennas, especially in terms of correlation between the stimulated and radiated pulses are investigated in [5], [6], [7], [8], [9], [10], [11], [12], [13], [14], and [15]. The fidelity factor and the pulse width stretch ratio are the two metrics to evaluate the pulse preservation performance. Do-Hoon Kwon in [16] has shown how the variation of the antenna gain and group delay affect these two factors. The investigation is based on a theoretical analysis and no particular antenna is studied, however, it is shown constant gain and group delay result in preserving the shape of the pulse.

In [6] and [17] the radiation and reception characteristics of some well known types of UWB antenna are studied. In these works, it is mentioned how different operating modes, transmitting and receiving, can results in having different pulse shapes. Moreover, it is concluded which types are not dispersive and which ones are. Although in these works the main focus is on the boresight and the performance of the antennas are judged based on that, in the latter work, it is shown that the pulse width and amplitude of the received pulse vary with the angle of incident.

Some researchers investigated not only on the boresight but on the principal planes as well. In [18] a printed circular disk monopole having different ground plane structures is studied. It is shown that having curved, and hexagonal ground planes can improve the correlation factor. A planar dipole is optimized in [10] to radiate similar pulses in the *E-plane*. Additionally, in [9] an UWB discone antenna is reported with having an almost identical Impulse Response (IR) in the *E-plane*.

Moreover, it appears that transient analysis of UWB Dielectric Resonator Antennas (DRAs) is not as popular as the one for the conventional types in the community. Nevertheless, [19], [20] reported interesting transient properties of rectangular UWB stacked DRAs. Excellent correlation factor for the angles besides the principal cuts, could be considered as the unique feature of this type of UWB antenna.

Despite the sophisticated literature that exists for UWB antennas, our research reveals no complete design guidelines on achieving a broadband antenna with a uniform ADD. Therefore, a broadband Dielectric Resonator Antenna (DRA) is proposed to satisfy the abovementioned characteristic.

The remainder of this paper is divided into five sections, where Section II provides the background theory and the guidelines. In Section III a proposed antenna is provided. The simulated and measured ADD results of the proposed antenna are shown in Section IV. Finally, the work is concluded in Section VI.

II. BACKGROUND THEORY AND THE GUIDELINES

Consider the scenario shown in Figure 3. In this configuration, the Tx sends signals to the Rx; from the same distance but different angles. Depending on the structure of the Rx, the received pulses from different angles, reach the port of the Rx at different time instants. To have a uniform ADD, the differences of these time instants need to be

[1]This is true for the Tx too, however, for our analysis Rx is sufficient.

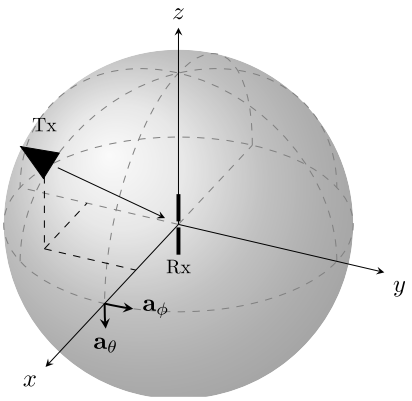

FIGURE 3. The configuration of Tx and Rx in the spherical coordinate system (far-field assumption).

negligible. With having some design consideration, a uniform ADD for a particular region can be achieved. Therefore, this section provides the background theory and the design guidelines for this purpose.

Consider a thin dipole antenna with length ℓ, as shown in Figure 4a. The antenna is impulsively excited. The signal has a width of σ and $\sigma < \tau_{l/2}$. $\tau_{l/2}$ is the time required for the signal to travel the length of a single arm of the dipole. In this case, there are three different sources of radiation. The radiated pulses from the two ends experience a 180° phase shift and are inverted versions of the excitation pulse. A thorough explanation of this scenario is provided by H. G. Schantz in [5, Ch. 5.3]. The radiated signal at an observation angle, will be the superposition of these three radiated signals, as illustrated in Figure 4b. Due to the geometry of the thin dipole antenna, the signals will be added constructively or destructively at different observation angles. Schantz shows if an antenna is designed in a way that the radiated pulses from different sources are always added constructively, the shape of the radiated signal will show better pulse preservation properties. Additionally, a circular planar dipole antenna is an example for this claim. This is because all the signals from different radiation sources travel similar distance to the observation point [5, Ch. 5.3.2.2] (for more information refer to the five rules in [21]).

With the help of signal and system theory, the relation between the input signal $x(t)$ and radiated signal $y(t, \theta, \phi)$ in time domain is

$$y(t, \theta, \phi) = x(t) * h(t, \theta, \phi) \tag{1}$$

where $(*)$ represents convolution operation and $h(t, \theta, \phi)$ is the angular dependent IR: θ and ϕ are co-elevation and azimuth angles, respectively.

Therefore, it can be concluded that the IR of an antenna for a particular angle is related to the number of radiation sources and their positions on the antenna.

For the radiated signal to be the same as the input signal, Eq. 1 suggests that IR, $h(t, \theta, \phi)$, would have to be a Dirac delta function. Additionally, it shows if the IR is the same for all the angles (not necessary a delta function), the radiated

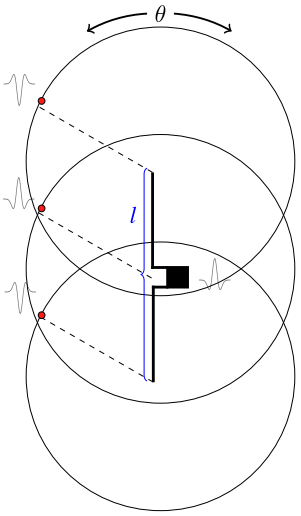

(a) Finite thin-wire dipole antenna stimulated with a *Gaussia W* pulse

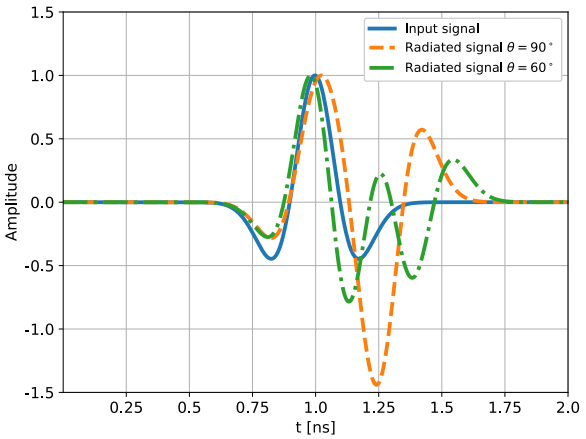

(b) Normalized radiated pulses from the thin-wire dipole antenna at different look angles

FIGURE 4. Input and output pulses of a thin dipole antenna.

pulses are the same for all the angles, although it can be different from the input signal. Therefore, in this case the performance of the antenna would be the same in all directions.

Assume the Antenna Under Test (AUT) in Figure 3 has identical IR for a particular region in the angular domain, say $\theta_1 \leq \theta \leq \theta_2$ and $\phi_1 \leq \phi \leq \phi_2$. In that case, the transmitted pulses from the Tx reach the port of the AUT at the same time instant, regardless of the Angle of Arrival (AoA) in that region.

Thus, the objective is to have identical IR for all the angles in a particular region. To achieve this, the following analyses are beneficial:

- Diffraction: If the structure of an antenna causes diffraction towards some angles, it is intuitive that the radiated pulses from the antenna experience different propagation delays towards those observation points. Therefore, any structure which can cause diffraction in the field of view should be avoided.
- Dimensions and shape: When the size of an antenna is big and not symmetric w.r.t the look angles, the radiated signals from the sources on the antenna, take different

paths to the observation angle. Therefore, to reduce the path difference for different radiating sources, the size of the antenna should be small. Moreover, it is desired to reduce the number of the radiating sources. Therefore, discontinuity and bends should be avoided.

- Phase center: An antenna with a constant phase center has the same radiation pattern at different frequencies within the operating BW. To achieve this, higher modes should not be excited. When the higher modes are excited, this results in having different radiation patterns at different frequencies. In other words, the lower-frequency and the higher-frequency components need to be radiated from the same part of the antenna. However, it should be noted, not exciting the higher modes will limit the impedance BW.

Based on these analyses, within the existing types of antenna, DRA is a good candidate to simultaneously meet all the requirements. In the next section a DRA with the required characteristics is proposed.

III. THE PROPOSED ANTENNA

A. DESIGN AND SIMULATION RESULTS

Dielectric Resonator (DR) with high permittivity is widely used in microwave circuits due to its high Q-factor. The high ϵ_r causes the majority of the energy to be confined in the DR, and the rest will be dissipated as radiation. However, the BW of the radiation would be narrow. To increase the BW, the Q-factor needs to be reduced. And if carefully designed, a DR can be turned into an antenna; known as DRA [22], [23], [24], [25]. DRAs possess some interesting characteristics which could help us to achieve our goal.

In case of DRA, electromagnetic modes are excited inside the DR. These modes result in standing waves, and they alternate (bounce forth and back) within the structure. At the resonant frequencies, the walls of the DR appear to be transparent to the waves, and they emerge, so radiation occurs [26, Ch. 1]. This unique radiation mechanism can be advantageous to have the phase center of the antenna as constant as possible, provided only the fundamental mode is excited.

The main dimension of a DRA is inversely proportional to $\sqrt{\epsilon_r}$. Therefore, a DR with a high ϵ_r, results in a short λ_g relative to λ_o, where λ_g and λ_o are guided and free space wavelengths, respectively. Therefore, the wavelength of the radiated electric field in the far-field is relatively larger than the wavelength of the wave inside the DR. From the observation point of view, this provides a tolerance for minor phase center displacement throughout the BW.

Thus, it is desired that the DRA to be as small as possible. However, a high permittivity reduces the impedance BW, therefore, a trade-off should be considered. In this work Al2O3 with dielectric constant of 9.8 and loss tangent of 0.003 is used.

Next, due to the thick block of dielectric materials used in DRA as the radiating element, fabrication is not an easy task, therefore, to ease the fabrication procedure, the simplest type

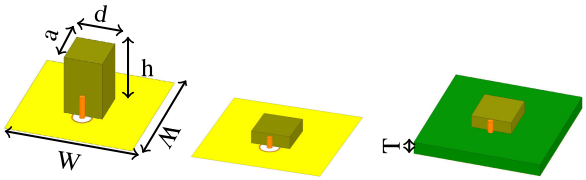

(a) Antenna I (b) Antenna II (c) Antenna III

FIGURE 5. DRAs with different configurations.

which is Rectangular Dielectric Resonator Antenna (RDRA), is chosen. For RDRA to have the main radiation in boresight, $TE_{11\delta}$ should be excited, where $\delta = [1, 3, 5, \ldots]$. This can be achieved by different feeding methods such as: probe, slot and microstrip line. For our investigation purposes center frequency of 6.5 GHz is selected.

To design a RDRA for TE^y_{111} mode, the following equations can be used [27]

$$k_x = \frac{\pi}{a}, \quad k_y = \frac{\pi}{b}, \quad \textit{and} \quad k_o = \frac{2\pi}{\lambda_o} \tag{2}$$

$$k_z \tan\left(\frac{k_z \cdot d}{2}\right) = \sqrt{(\epsilon_r - 1) \cdot k_o^2 - k_z^2} \tag{3}$$

$$k_x^2 + k_y^2 + k_z^2 = \epsilon_r \cdot k_o^2 \tag{4}$$

where k_x, k_y and k_z are the wavenumbers, k_o is the free-space wavenumber of the resonant frequency, a, d and b are the length, width and height of the DR, respectively. The equations are for an isolated RDRA, however, with the presence of the ground plane the height should be halved, $h = \frac{b}{2}$. For a = d = 9 mm and h = 14.5 mm, the theoretical resonant frequency is 6.508 GHz.

A RDRA with the abovementioned dimensions and dielectric constant is designed in HFSS. The antenna is shown in Figure 5a. To ease the fabrication procedure and achieving a broadband performance, probe feeding technique is used. Additionally, to avoid drilling the radiating DR, the probe is placed adjacent to the DR and positioned in the middle to have the maximum coupling [27]. The predicted resonant frequency using HFSS is 6.422 GHz. The error of theoretical and simulated results is about 1.3%. Since the DR has a tall height relative to its base dimensions, it supports TE^y_{113} mode as well (refer to [28]). Since both modes TE^y_{111} and TE^y_{113} are excited in Antenna I, a very wide impedance BW is achieved, as illustrated in Figure 6.

However, excitation of TE^y_{113} mode is not of interest. This is because, the guidelines in Section II suggest that the higher modes should not be excited. Therefore, not only we do not benefit from the tall height, it could even have a negative impact on the phase center variation over the frequency and the look-up angles, and limiting the field-of-view which has uniform ADD. Thus, it is desired to reduce the height of the block so that, only TE^y_{111} mode is excited, yet the broadband requirement is met.

To achieve a high BW, there are various techniques as discussed in [25, Ch. 5]. However, they do not satisfy all the requirements simultaneously. For example,

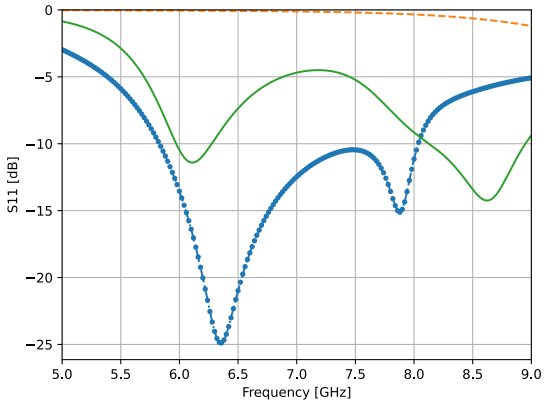

FIGURE 6. Return loss of the antennas in Figures 5. Dotted dashed: Antenna I, dashed: Antenna II, solid: Antenna III.

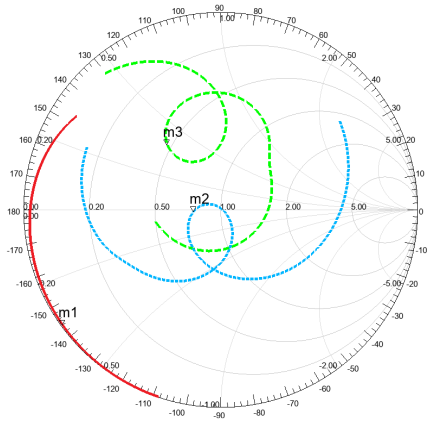

FIGURE 7. Load impedance: solid: Antenna II, long dashed: Antenna III, dashed: the proposed antenna. All the markers indicate 6.5GHz.

multi-stacking which is a very popular technique, leads to having multi-resonance since multiple DRs with different values of ϵ_r are needed. Another approach is to use a thick substrate between the radiating DR and the ground plane, this approach is reported in [29] although multi-resonance behavior is observed. With having a thick substrate the losses increase and this reduces the Q-factor and results in a wider impedance BW. For the proposed antenna the latter technique is used.

To keep the size of the radiating DR small, the based dimensions are unchanged. A substrate between the DR and the ground plane is inserted. To determine the height of the substrate, two design parameters are fixed to ease the analysis, the height of the DR, h is set to be 3 mm and the same material as the one for DR is used for the substrate. To have a low profile antenna we introduced a height constrain as

$$\frac{1}{3}a \leq H \leq \frac{2}{3}a$$

where $\mathrm{H} = T + h$.

Based on the constrain, the minimum and maximum values for T are 0 and 3 mm, respectively. Furthermore, 2 RDRAs are designed based on the new configurations: 1) Without substrate: a DR with the dimensions of $9 \times 9 \times 3\,\mathrm{mm}^3$ over a

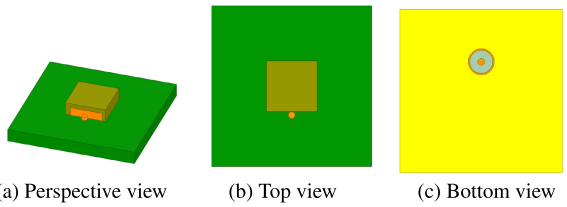

FIGURE 8. The proposed DRA with a square ground plane.

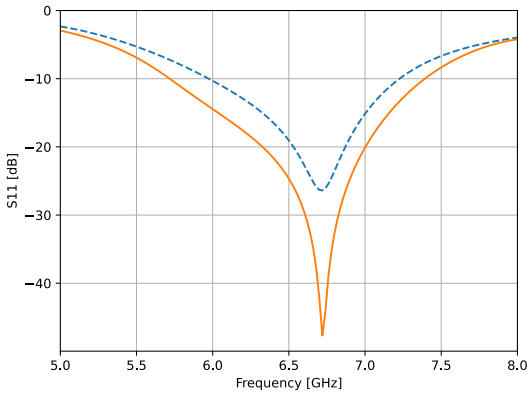

FIGURE 9. The proposed DRA. Dashed line: with square ground plane, solid line: with elliptical ground plane

ground plane, 2) With substrate: a DR with the dimensions of $9 \times 9 \times 3\,\mathrm{mm}^3$ is place over a substrate with the dimensions of $30 \times 30 \times 3\,\mathrm{mm}^3$, as shown in Figure 5b and 5c, respectively.

The return loss of the 2 antennas are shown in Figure 6. It can be seen that Antenna II without a substrate does not resonate at the desired frequency. However, inserting the substrate causes Antenna III to resonate at the desired frequency. However, both modes TE^y_{111} and TE^y_{113} are excited. Additionally, the impedance BW for TE^y_{111} is not sufficient.

The load impedance of the antennas are shown in Figure 7. To have a good matching for the antenna with the substrate, either a shunt capacitor or a combination of series capacitor and a shunt inductor can be used. Therefore, a metallic strip is added to the feeding probe of Antenna III. The dimensions of the strip are tuned, so that, the center frequency is moved near to the center of the Smith chart to match TE^y_{111} and move the TE^y_{113} away from the center. That results in the configuration of the proposed antenna, and it is shown in Figure 8. The matching line has a length of $mL = 7.5$ mm and a height of $mH = 2.5$ mm.

Throughout the whole investigation, size of the ground plane is fixed to $W \times W = 30 \times 30\,\mathrm{mm}^2$, the diameter of the probe is $pD = 1$ mm and the thickness of the conducting sheet is $t = 0.006$ mm.

The proposed antenna operates from 6 GHz to 7.5 GHz and there is only a single dip presented within the -10 dB BW. The load impedance and return loss of the proposed antenna are shown in Figure 7 and 9, respectively. The antenna satisfies the minimum required fractional BW for UWB.

The radiation patterns of the antenna for different frequencies are illustrated in Figure 10. The antenna has a realized

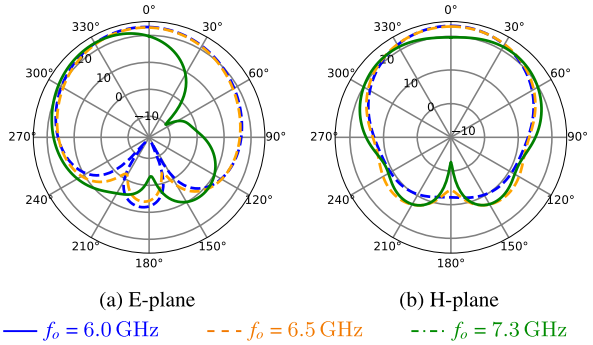

FIGURE 10. Electric field radiation patterns of the proposed antenna with square ground plane [dB].

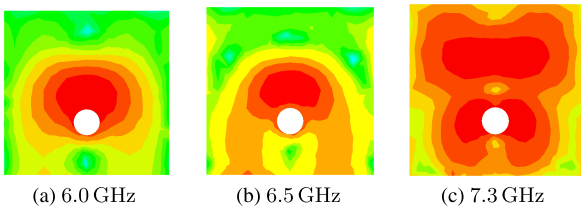

FIGURE 11. Current distribution on the square ground plane.

gain of 5.2 dBi in the boresight. It can be seen that the radiation pattern is almost constant in the H-plane over the whole frequency band and a minor gain reduction happens at the upper frequencies. However, in the E-plane at the upper frequency band the radiation pattern degrades and a null starts to appear about 60°. This is not due to the higher modes, as they are not excited in DR, but the null is due to the ground plane.

The corners of the ground plane contribute to this. At lower frequency band the electrical current is distributed fairly uniformly on the ground plane. However, the current starts to flow towards the corners as the frequency increases, as shown in Figure 11. This introduces a minor null on the ground plane as depicted in Figure 11c. Therefore, throughout the impedance BW the effect of the ground plane varies, and its corners act as extra radiating sources and results in destructive superpositions. To solve this problem, we can use an elliptical ground plane.

As the frequency increases, electrical current tends to travel at the edges of a conducting sheet (the skin effect) [30], [31]. To keep the current distribution on the edges of the ground plane as uniform as possible, an elliptical ground plane is proposed in this work. This is because, there are no sharp edges that results in charge accumulation. The shape of the ground plane for the proposed antenna is modified to an elliptical shape. All the other parameters remained the same. It should be noted that the circular cutout on the ground plane affects the current distribution, therefore, if the shape and location of the cutout changes, it is not confirmed that an elliptical ground plane is optimum.

The configuration of the DRA with elliptical ground plane and its return loss are presented in Figure 12 and in Figure 9,

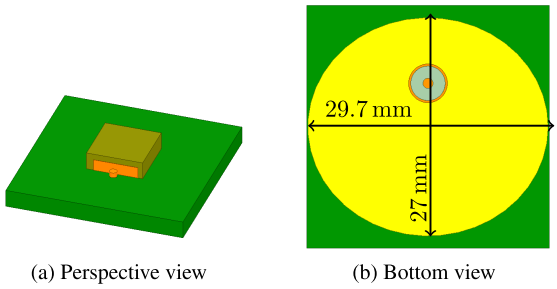

FIGURE 12. The proposed DRA with an elliptical ground plane.

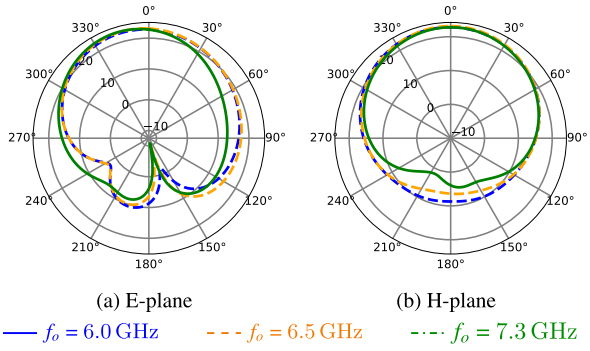

FIGURE 13. Electric field radiation patterns of the proposed antenna with elliptical ground plane [dB].

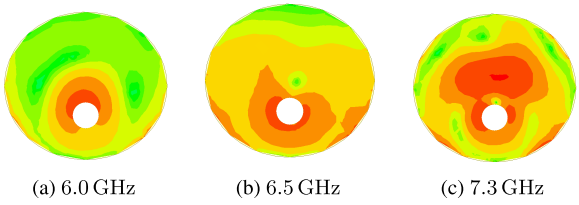

FIGURE 14. Current distribution on the elliptical ground plane.

respectively. The ratio of the minor to major axis of the ellipse is tuned to obtain the optimized performance. The elliptical ground plane increases the impedance BW of the antenna compared to the one with a rectangular ground plane. The radiation patterns of the DRA with an elliptical ground plane are shown in Figure 13. It can be seen that there is no null in the radiation pattern at $\theta = 60°$. The current distribution on the elliptical ground plane for different frequencies are shown in Figure 14.

B. FABRICATION AND PRACTICAL RESULTS

To verify the simulated results the proposed antennas are fabricated and measured. The fabricated antennas are shown in Figure 15. The measured return loss of the antennas are shown in Figure 16. The DRA with an elliptical ground plane resonates at the desired frequency.

For having a better comparison between the two different antennas, the normalized radiation patterns are shown in Figure 17.

In Table 1 the comparison of the simulated and the measured realized gain for boresight are provided. There is a

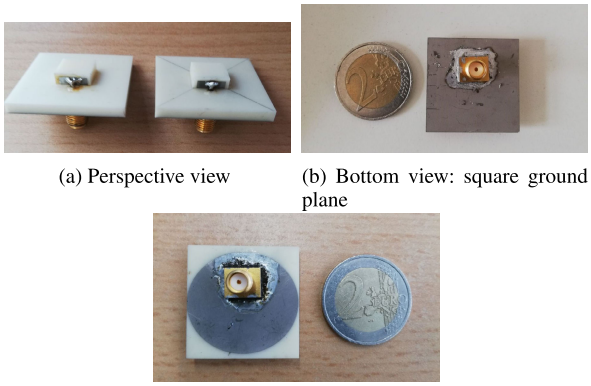

(a) Perspective view (b) Bottom view: square ground plane

(c) Bottom view: elliptical ground plane

FIGURE 15. The proposed fabricated DRAs.

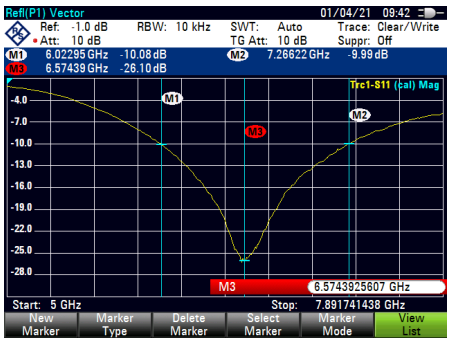

(a) DRA with square ground plane

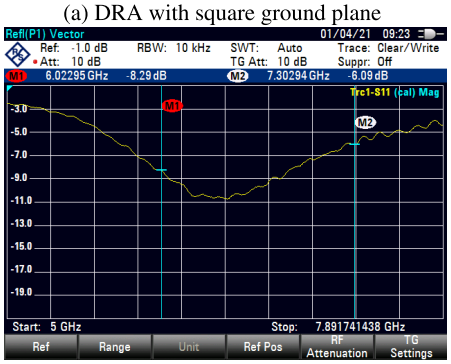

(b) DRA with elliptical ground plane

FIGURE 16. Measured return loss.

good agreement between the practical and simulated results. The DRA with an elliptical ground plane is selected for further procedure.

IV. RESULTS AND DISCUSSION

This section provides the radiated pulses and the ADD for the proposed antenna with an elliptical ground plane. To obtain the radiated pulses and estimating the delay, the frequency domain approach in [3] is used. This approach requires the full polarimetric complex transfer function of the antenna. *HFSS* is used to obtain the simulated required data. In simulation the proposed antenna is in Tx mode. And the practical data is obtained in anechoic chamber, with having the proposed antenna in Rx mode, and a *DRH10* reference antenna as the transmitter.

TABLE 1. Comparison of realized gain of the proposed antennas.

f_o (GHz)	6.0	6.5	7.3
Simulated: Square GND (dBi)	5.38	5.20	2.04
Measured: Square GND (dBi)	5.40	5.47	0.07
Simulated: elliptical GND (dBi)	5.00	5.34	4.93
Measured: elliptical GND (dBi)	4.92	5.66	4.65

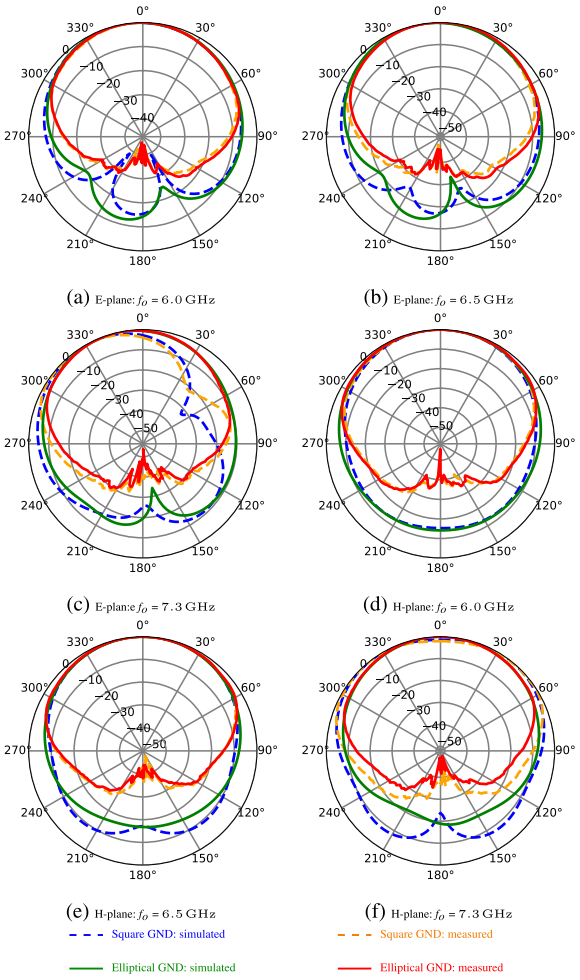

FIGURE 17. Normalized radiation patterns of the proposed antennas for the E- and H-planes [dB].

A. RADIATED PULSE

1) SIMULATED RADIATED PULSE

To obtain the radiated pulse for different angles, a broadband pulse is created. The pulse is a modulated Gaussian pulse with a BW of 1.3 GHz, from 6.0 GHz to 7.3 GHz. It should

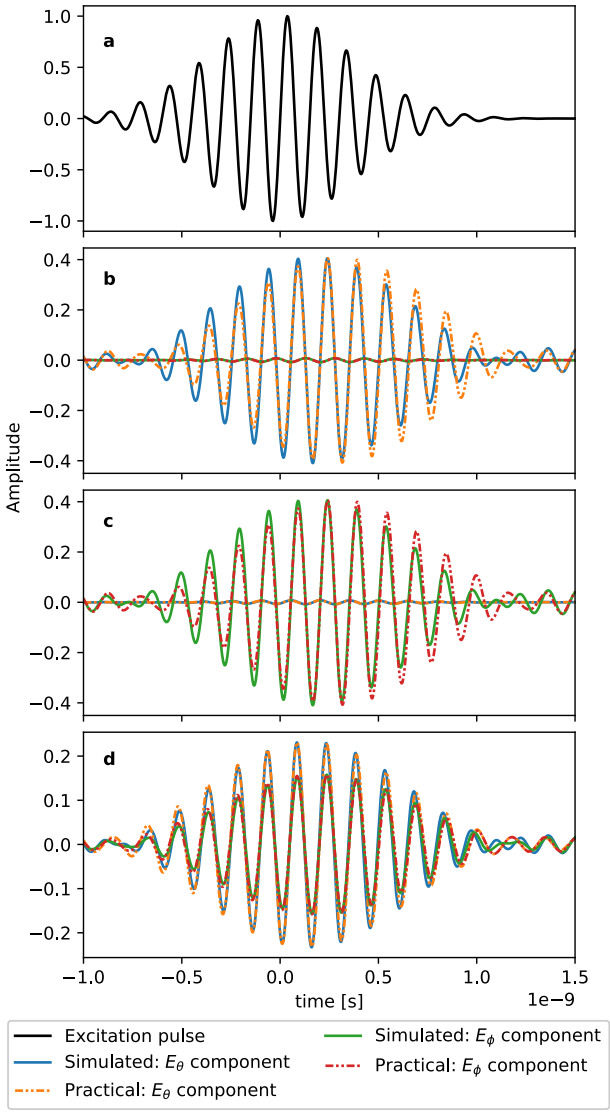

FIGURE 18. (a) is the excitation pulse, and (b)-(d) are the radiated pulses for $E(\theta, \phi) = (0°, 0°)$, $(0°, 90°)$, and $(45°, 45°)$, respectively. Practical pulses are normalized w.r.t their corresponding simulated pulses.

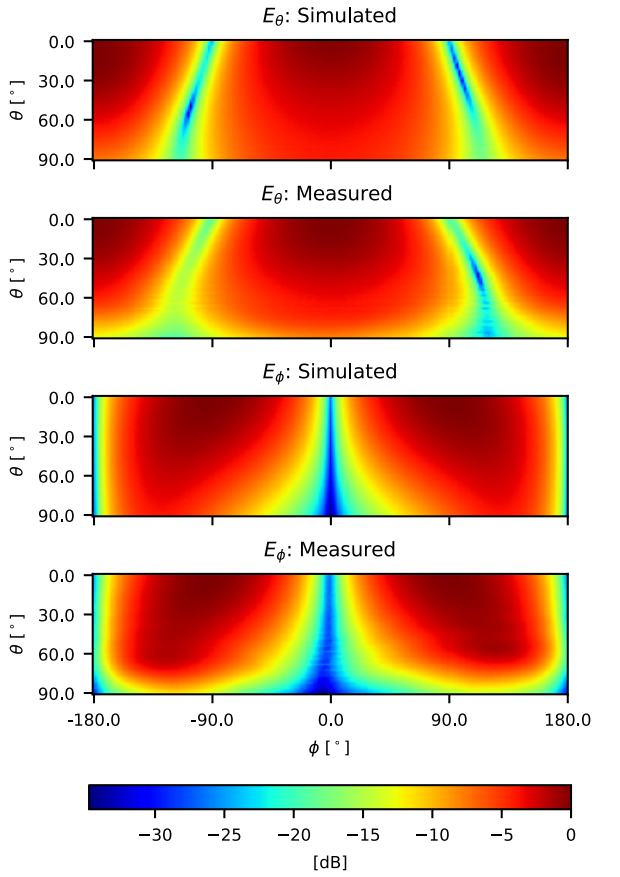

FIGURE 19. Normalized Radiation patterns for the upper-hemisphere at $f = 6.5$ GHz. This figure illustrates in which regions the antenna possesses nulls throughout the operating BW.

be noted that duration of the Gaussian pulse (before the modulation), corresponds to its 10 dB BW spectrum.

To obtain the radiated pulse, the spectrum of the excitation pulse is multiplied with the transfer function of the antenna for an angle of interest. Then, Inverse Fourier Transform (IFT) is performed on the resultant spectrum. The result of the IFT is the radiated pulse. The excitation pulse and the radiated pulses are shown in Figure 18.

2) PRACTICAL RADIATED PULSE

To obtain the practical radiated pules, two extra post-processing steps must be performed compared to the one in the simulated scenario. First, the transfer functions of the transmitting antenna (reference antennas) and the channel (free space) must be de-embedded from the insertion loss (S_{21}) between the Tx and the AUT. Therefore, $H_{\mathrm{Rx}} = S_{21} \cdot H_{\mathrm{ch}}^{-1} \cdot H_{\mathrm{Tx}}^{-1}$.

Second, the proposed antenna in measurement is in Rx mode as mentioned earlier. Therefore, to have the radiated pulses, the antenna should have been in Tx mode, thus H_{Tx} of the AUT is required. This can be easily achieved with applying *Lorentz's reciprocity*. The theorem claims $H_{\mathrm{Tx}} = j/\lambda \cdot H_{\mathrm{Rx}}$ [32], [33], [34], [35]. With having it applied, the transfer function of the AUT in Tx mode can be obtained. Then, the rest of the procedure is the same as the one in the simulated scenario.

Figure 18 shows that the shapes of radiated pulses for different angles are preserved, and the radiated pulses are almost identical to the input pulse. This supports the argument that is established in Section II.

B. ADD ESTIMATION

With having the full polarimetric complex transfer function of the antenna, as described in [3], the delay that is induced by the proposed antenna for every angle can be estimated. To have a better understanding about the estimated ADD, the radiation patterns of the antenna for $|E_\theta|$ and $|E_\phi|$ at operating frequency of 6.5 GHz are shown in Figure 19. With considering the mounting position which limits the antenna's field-of-view to the upper hemisphere, radiation patterns in Figure 19 illustrate only the upper hemisphere,

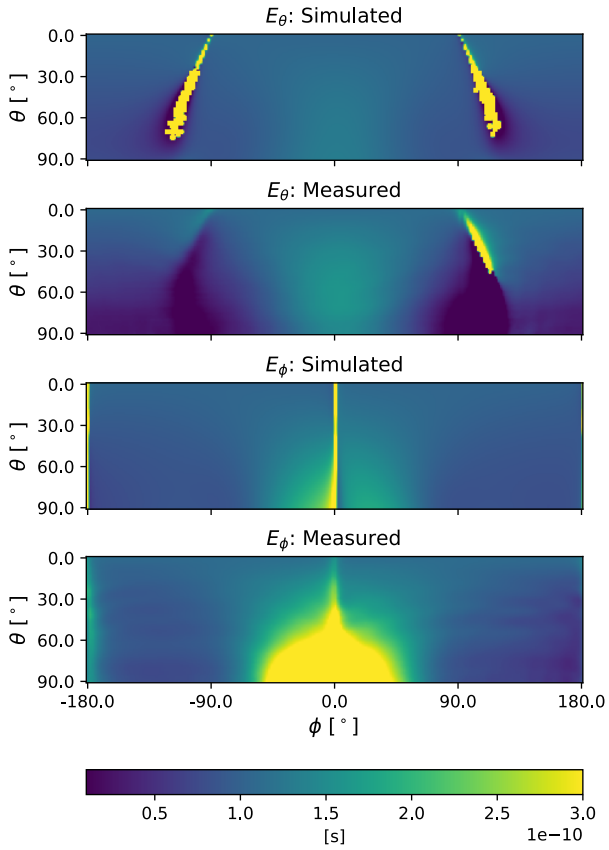

FIGURE 20. Estimated ADD.

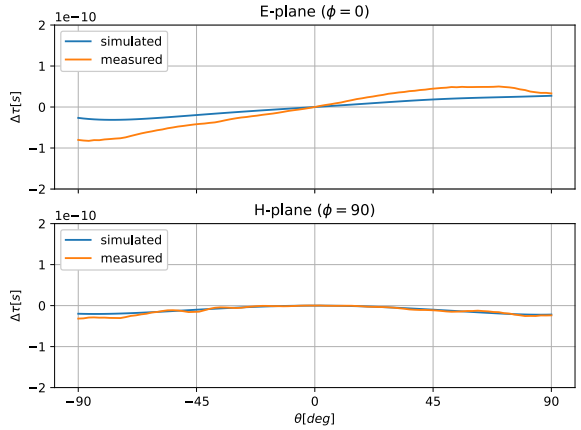

FIGURE 21. Estimated ADD for *E-plane* and *H-plane* relative to the boresight.

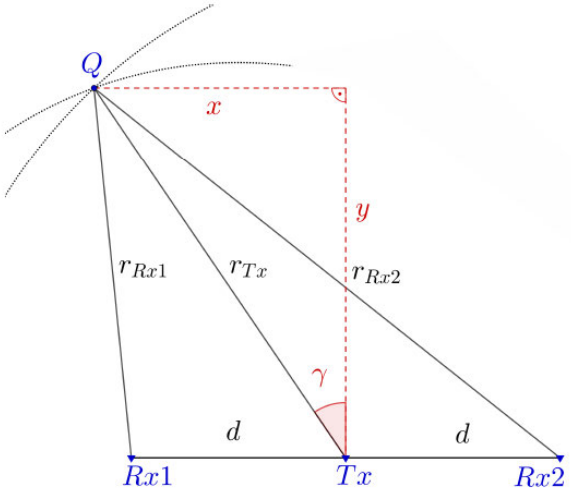

FIGURE 22. Position estimation with indicated intersection of the ellipses [36].

as the lower hemisphere is not of interest. Although the radiation patterns of a single frequency is shown here, this is sufficient to illustrate in which regions the antenna possesses nulls. In those regions as well as their proximities, a precise ADD estimation should not be expected. It would be either too high or too low.

The estimated ADD is shown in Figure 20. There is a good agreement between the simulated and measured results. The results suggest the antenna induces almost a uniform delay in the upper hemisphere.

To have a closer look, the estimated delays for the *E-plane* and the *H-plane* are plotted in Figure 21. To illustrate the relative delay w.r.t the boresight, the results are shifted that boresight is placed at 0 s. The practical estimated delay for H-plane is almost the same as the one for simulated. The highest delay occurs at boresight and the antenna induces lesser delay as the angle moves toward the sides. The maximum delay for the simulated scenario is about 21 ps, and it is symmetrical. The result for the practical scenario agrees strongly with the simulated results. However, there is a difference of 11 ps around $\theta = -90°$.

However, for the E-plane case, the results are not symmetrical. This due to the existence of the feeding probe and the matching line, therefore, perfectly symmetrical ADD for E_θ cannot be obtained if single probe-fed approach is used. Compared to the boresight, the antenna induces a greater delay towards $\theta = +90°$ (the right side) and lesser delay towards $\theta = -90°$ (the left side). On the right side the maximum delay for the simulated scenario is 27.5 ps and on the left side is 31.3 ps. The practical result for the E-plane has the same behavior as the one for the simulated, however the agreement between the two is not as strong as the one for the H-plane. The maximum delays for the measured results on the righ and the left sides are 34.5 ps and 82.6 ps, respectively. There is about 50 ps difference between the practical and simulated results for the E-plane. This outcome suggests that the accuracy of estimating the ADD is closely linked to the sensitivity of the phase measurement.

V. TIME DIFFERENCE OF ARRIVAL

To evaluate the performance of the proposed antenna regarding TDoA estimation, consider the scenario depicted in Figure 22. In an ideal case, the propagation delay is unaffected by the Rx antennas. As a result, the true position of the target can be calculated. By replacing the Rx antennas

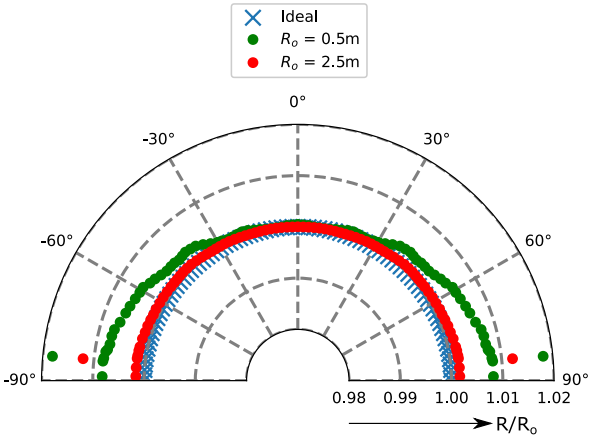

FIGURE 23. Comparison between the true and estimated positions of the target at different distances .

with the proposed antenna, we can subsequently gauge the antenna's effectiveness.

For our purpose the practical results for the H-plane of the antenna is used. In Figure 23 a comparison between the true position of the target and the estimated position at different distances are presented. For $r_{T_x} = 0.5\,\text{m}$ the estimated and true values are almost identical for $-30° \leq \theta \leq +30°$. Beyond this region estimation error start to appear however, it is not significant. For example, at $\theta = 60°$ the estimation error for the range is 1.24 mm, and for the angle, it is 0.26°. As the distance to the target increases, the estimation error decreases. When r_{T_x} is 2.5 m these values reduce to 0.3 mm and 0.11°, respectively.

The estimated results suggest that since the error caused by the antenna's imperfection is negligible, the localization can be performed without requiring a calibration step. Furthermore, taking into account the estimated ADD shown in Figure 20, it is possible to omit a calibration step for the upper hemisphere.

VI. CONCLUSION

This contribution provides a broadband DRA with a uniform ADD for the upper hemisphere. The proposed antenna is validated experimentally. It is concluded that if a uniform ADD over the upper hemisphere is desired, having constant radiation patterns within the impedance BW is the main factor to achieve this goal. This limits the operating BW as the higher modes should not be excited.

Finally, we have shown that the proposed DRA can be used successfully for indoor localization without the need for a calibration step.

ACKNOWLEDGMENT

The author Ali Rashidifar would like to thank Dr. Hans G. Schantz and Dr. Jürgen Sachs for the insightful discussions. In addition, thanks to Michael Huhn a member of HMT Group, TU Ilmenau, for his help during the measurement in the anechoic chamber.

REFERENCES

[1] C. Smeenk, T. E. Wegner, G. Kropp, J. Trabert, and G. D. Galdo, "Localization and navigation of service robots by means of M-sequence UWB radars," in *Proc. 18th Eur. Radar Conf. (EuRAD)*, Apr. 2022, pp. 189–192, doi: 10.23919/EuRAD50154.2022.9784511.

[2] S. Gezici, Z. Tian, G. B. Giannakis, H. Kobayashi, A. F. Molisch, H. V. Poor, and Z. Sahinoglu, "Localization via ultra-wideband radios: A look at positioning aspects for future sensor networks," *IEEE Signal Process. Mag.*, vol. 22, no. 4, pp. 70–84, Jul. 2005, doi: 10.1109/MSP.2005.1458289.

[3] A. Rashidifar, S. Semper, and C. W. Wagner, "A frequency domain approach for estimating the angular dependent delay of an UWB antenna," in *Proc. 16th Eur. Conf. Antennas Propag. (EuCAP)*, Mar. 2022, pp. 1–5, doi: 10.23919/EuCAP53622.2022.9769534.

[4] J. Sachs, *Handbook of Ultra-Wideband Short-Range Sensing: Theory, Sensors, Applications*. Hoboken, NJ, USA: Wiley, 2013.

[5] H. Schantz, *The Art and Science of Ultrawideband Antennas* (Artech House Antennas and Electromagnetics Analysis Library). Norwood, MA, USA: Artech House, 2015.

[6] D. Ghosh, A. De, M. C. Taylor, T. K. Sarkar, M. C. Wicks, and E. L. Mokole, "Transmission and reception by ultra-wideband (UWB) antennas," *IEEE Antennas Propag. Mag.*, vol. 48, no. 5, pp. 67–99, Oct. 2006, doi: 10.1109/MAP.2006.277157.

[7] W. Wiesbeck, G. Adamiuk, and C. Sturm, "Basic properties and design principles of UWB antennas," *Proc. IEEE*, vol. 97, no. 2, pp. 372–385, Feb. 2009, doi: 10.1109/JPROC.2008.2008838.

[8] E. Pancera, T. Zwick, and W. Wiesbeck, "Spherical fidelity patterns of UWB antennas," *IEEE Trans. Antennas Propag.*, vol. 59, no. 6, pp. 2111–2119, Jun. 2011, doi: 10.1109/TAP.2011.2143666.

[9] N. Rostomyan, A. T. Ott, R. Brem, C. J. Eisner, and T. F. Eibert, "A compact balanced symmetric discone antenna with optimized ultra-wideband omnidirectional impulse radiation behavior," in *Proc. 8th Eur. Conf. Antennas Propag. (EuCAP)*, Apr. 2014, pp. 83–86, doi: 10.1109/EuCAP.2014.6901698.

[10] P. Cerny and M. Mazanek, "Optimized ultra wideband dipole antenna," in *Proc. 18th Int. Conf. Appl. Electromagn. Commun.*, 2005, pp. 1–4, doi: 10.1109/icecom.2005.205035.

[11] A. H. Mohammadian, A. Rajkotia, and S. S. Soliman, "Characterization of UWB transmit-receive antenna system," in *Proc. IEEE Conf. Ultra Wideband Syst. Technol.*, Jun. 2003, pp. 157–161, doi: 10.1109/UWBST.2003.1267823.

[12] S.-G. Mao and S.-L. Chen, "Frequency- and time-domain characterizations of ultrawideband tapered loop antennas," *IEEE Trans. Antennas Propag.*, vol. 55, no. 12, pp. 3698–3701, Dec. 2007, doi: 10.1109/TAP.2007.910494.

[13] K. Kikuta and A. Hirose, "Dispersion characteristics of ultra wideband antennas and their radiation patterns," in *Proc. Int. Symp. Electromagn. Theory*, May 2013, pp. 462–465.

[14] M. N. Hasan, O. J. Babarinde, S. Das, and K. V. Babu, "Dispersion characterization of a UWB Vivaldi antenna in time and frequency domain," in *Proc. IEEE Indian Conf. Antennas Propogation (InCAP)*, Dec. 2018, pp. 1–4, doi: 10.1109/INCAP.2018.8770763.

[15] Z. N. Low, J. H. Cheong, and C. L. Law, "Low-cost PCB antenna for UWB applications," *IEEE Antennas Wireless Propag. Lett.*, vol. 4, pp. 237–239, 2005, doi: 10.1109/LAWP.2005.852577.

[16] D.-H. Kwon, "Effect of antenna gain and group delay variations on pulse-preserving capabilities of ultrawideband antennas," *IEEE Trans. Antennas Propag.*, vol. 54, no. 8, pp. 2208–2215, Aug. 2006, doi: 10.1109/TAP.2006.879189.

[17] K. Rambabu, A. E. Tan, K. K. Chan, and M. Y. Chia, "Estimation of antenna effect on ultra-wideband pulse shape in transmission and reception," *IEEE Trans. Electromagn. Compat.*, vol. 51, no. 3, pp. 604–610, Aug. 2009, doi: 10.1109/TEMC.2009.2023364.

[18] Q. Wu, R. Jin, J. Geng, and M. Ding, "Pulse preserving capabilities of printed circular disk monopole antennas with different grounds for the specified input signal forms," *IEEE Trans. Antennas Propag.*, vol. 55, no. 10, pp. 2866–2873, Oct. 2007, doi: 10.1109/TAP.2007.905854.

[19] M. S. Iqbal and K. P. Esselle, "Pulse performance of a UWB dielectric resonator antenna," in *Proc. IEEE Antennas Propag. Soc. Int. Symp. (APSURSI)*, Jul. 2014, pp. 1982–1983, doi: 10.1109/APS.2014.6905318.

[20] M. Shahzad Iqbal and K. P. Esselle, "Pulse-preserving characteristics and effective isotropically radiated power spectra of a new ultrawideband dielectric resonator antenna," *IET Microw., Antennas Propag.*, vol. 12, no. 7, pp. 1231–1238, Jun. 2018, doi: 10.1049/iet-map.2017.0172.
[21] H. G. Schantz, "Dispersion and UWB antennas," in *Proc. Int. Workshop Ultra Wideband Syst. Joint Conf. Ultra Wideband Syst. Technol., Joint UWBST IWUWBS*, Aug. 2004, pp. 161–165.
[22] R. D. Richtmyer, "Dielectric resonators," *J. Appl. Phys.*, vol. 10, no. 6, pp. 391–398, Jun. 1939, doi: 10.1063/1.1707320.
[23] M. Gastine, L. Courtois, and J. L. Dormann, "Electromagnetic resonances of free dielectric spheres," *IEEE Trans. Microw. Theory Techn.*, vol. MTT-15, no. 12, pp. 694–700, Dec. 1967, doi: 10.1109/TMTT.1967.1126568.
[24] D. Kajfez and P. Guillon, *Dielectric Resonators* (Artech House Microwave Library). New York, NY, USA: Noble, 1998.
[25] K. M. Luk and K. W. Leung, *Dielectric Resonator Antennas* (Antennas Series). Hertfordshire, U.K.: Research Studies Press, 2003.
[26] R. S. Yaduvanshi and H. Parthasarathy, *Rectangular Dielectric Resonator Antennas: Theory and Design*. India: Springer, 2015.
[27] R. Kumar Mongia and A. Ittipiboon, "Theoretical and experimental investigations on rectangular dielectric resonator antennas," *IEEE Trans. Antennas Propag.*, vol. 45, no. 9, pp. 1348–1356, Nov. 1997, doi: 10.1109/8.623123.
[28] X. Sheng Fang, C. Kin Chow, K. Wa Leung, and E. Hock Lim, "New single-/dual-mode design formulas of the rectangular dielectric resonator antenna using covariance matrix adaptation evolutionary strategy," *IEEE Antennas Wireless Propag. Lett.*, vol. 10, pp. 734–737, 2011, doi: 10.1109/LAWP.2011.2162389.
[29] N. Ojaroudiparchin, M. Shen, and G. F. Pedersen, "MM-wave dielectric resonator antenna (DRA) with wide bandwidth for the future wireless networks," in *Proc. 21st Int. Conf. Microw., Radar Wireless Commun. (MIKON)*, May 2016, pp. 1–4, doi: 10.1109/MIKON.2016.7492007.
[30] I. Pele, Y. Mahe, A. Chousseaud, S. Toutain, and P. Y. Garel, "Antenna design with control of radiation pattern and frequency bandwidth," in *Proc. IEEE Antennas Propag. Soc. Symp.*, Apr. 2004, pp. 783–786, doi: 10.1109/APS.2004.1329787.
[31] G. Lu, I. Korisch, L. Greenstein, and P. Spasojevic, "Antenna modelling using linear elements, with applications to UWB," in *Proc. IEEE Antennas Propag. Soc. Symp.*, vol. 3, Nov. 2004, pp. 2544–2547, doi: 10.1109/APS.2004.1331892.
[32] M. Kanda, "Time domain sensors for radiated impulsive measurements," *IEEE Trans. Antennas Propag.*, vol. AP-31, no. 3, pp. 438–444, May 1983, doi: 10.1109/TAP.1983.1143057.
[33] J. Kunisch, "Implications of Lorentz reciprocity for ultra-wideband antennas," in *Proc. IEEE Int. Conf. Ultra-Wideband*, Sep. 2007, pp. 214–219, doi: 10.1109/ICUWB.2007.4380944.
[34] Y. Duroc, T.-P. Vuong, and S. Tedjini, "A time/frequency model of ultrawideband antennas," *IEEE Trans. Antennas Propag.*, vol. 55, no. 8, pp. 2342–2350, Aug. 2007, doi: 10.1109/TAP.2007.901834.
[35] J. Kunisch and J. Pamp, "UWB radio channel modeling considerations," in *Proc. UWB Radio Conf.*, 2003, pp. 277–284.
[36] T. Hemmecke, "Sensordatenfusion von ultrabreitband-radar und tiefenkamera in der service-robotik," Dept. Electron. Meas. Signal Process. Group EMS TU Ilmenau, Diplomarbeit Technische Universitt Ilmenau, Ilmenau, Germany, Tech. Rep. 1831529394 at TU Ilmenau library, 2022.

ALI RASHIDIFAR received the degree in electronics engineering with a focus on microwave and telecommunications and the master's degree in communication and signal processing from Technische Universität Ilmenau (TU Ilmenau), in 2020. Since 2020, he has been a Research Assistant with the Electronic Measurements and Signal Processing Group, TU Ilmenau. His research interests include antenna design, antenna packaging and miniaturization, and antenna measurement and post-processing.

FLORIAN RÖMER (Senior Member, IEEE) received the Dr.-Ing. degree in electrical engineering from Technische Universität Ilmenau (TU Ilmenau), in 2012. From 2006 to 2012, he was a Research Assistant with the Communications Research Laboratory, TU Ilmenau. In 2012, he joined the Electronic Measurements and Signal Processing Group, a joint research activity between the Fraunhofer Institute for Integrated Circuits IIS and Ilmenau University of Technology, as a Postdoctoral Research Fellow. In January 2018, he joined the Fraunhofer Institute for Nondestructive Testing IZFP, where he is leading the SigMaSense Group with a research focus on innovative sensing and signal processing for nondestructive testing and has recently taken the role of the Chief Scientist leading the Center of Expertise on Applied AI, Signal Processing, and Data Analysis. From 2020 to 2022, he has served as an Associate Editor for IEEE TRANSACTIONS ON SIGNAL PROCESSING. Since 2022, he has been a Senior Area Editor.

SEBASTIAN SEMPER received the M.Sc. degree, in 2015, and the Ph.D. degree (Hons.) in electrical engineering, in 2022. He studied mathematics with Technische Universität Ilmenau (TU Ilmenau), Ilmenau, Germany. Since 2015, he has been a Research Assistant with the Electronic Measurements and Signal Processing Group, which is a joint research activity between the Fraunhofer Institute for Integrated Circuits IIS and TU Ilmenau. Since then, he has also been a Postdoctoral Student with the Electronic Measurements and Signal Processing Group, TU Ilmenau. In 2023, he spent six months with the Wireless Division, National Institute of Standards and Technology (NIST), Gaithersburg, MD, USA, where he worked on various channel sounding systems and related algorithms. His research interests include compressive sensing, parameter estimation, optimization, numerical methods, and algorithm design.

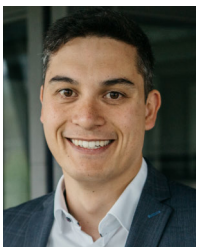

NAM GUTZEIT studied materials science in Ilmenau and Peru. He started his professional career in the field of electronics development based on low-temperature cofired ceramics (LTCC) with Ilmenau University of Technology, in 2011. He is the managing partner of eCeramix GmbH. He founded eCeramix GmbH together with three colleagues, in 2020. Since then, the team of eCeramix GmbH has developed and manufactured special electronics based on LTCC for sensor and packaging applications in the fields of biotechnology, automotive, aerospace, and high-frequency applications. The offered technologies for miniaturization of circuits enable the use of LTCC substrates in the field of semiconductor assembly or photonic technologies.

GIOVANNI DEL GALDO (Member, IEEE) received the Laurea degree in telecommunication engineering from Politecnico di Milano, Milan, Italy, and the Dr.-Ing. degree in MIMO channel modeling for mobile communications from Technische Universität Ilmenau, Ilmenau (TU Ilmenau), Germany, in 2007. Then, he joined the Fraunhofer Institute for Integrated Circuits IIS, Erlangen, Germany, focusing on audio watermarking and parametric representations of spatial sound. Since 2012, he has been leading a joint research group composed of the Fraunhofer Institute for Integrated Circuits IIS and a Full Professor with TU Ilmenau in the research area of electronic measurements and signal processing. Since 2017, he has been the Head of the Institute for Information Technology, TU Ilmenau. His current research interests include the analysis, modeling, and manipulation of multidimensional signals, over-the-air testing for terrestrial and satellite communication systems, and sparsity-promoting reconstruction methods.